Effect of hidden color channels on the nucleon-nucleon interaction

Hongxia Huang,[1] Pu Xu,[2] Jialun Ping,[1] and Fan Wang[3]

[1]*Department of Physics, Nanjing Normal University, Nanjing 210097, P.R. China*
[2]*Department of Applied Physics, Nanjing University of Science and Technology, Nanjing 210094, P.R. China*
[3]*Department of Physics, Nanjing University, Nanjing 210093, P.R. China*

In the framework of a constituent quark model, the effect of hidden color channels on the nucleon-nucleon (NN) interaction is studied. By adjusting the color confinement strength between the hidden color channels and color singlet channels and/or between the hidden color channels and hidden color channels, the experimental data of S- to I-partial-wave phase shifts of NN scattering can be fitted well. The results show that the hidden color channel coupling might be important in producing the intermediate-range attraction of the NN interaction. The deuteron properties and dibaryon candidates have also been studied with this model.

PACS number(s): 13.75.Cs, 12.39.Pn, 12.39.Jh, 21.30.−x

I. INTRODUCTION

The study of nucleon-nucleon (NN) interaction has lasted over 70 years. The quantitative description of NN interaction has been achieved in the one-boson-exchange (OBE) models [1], the chiral perturbation theory (ChPT) [2], and quark models [3].

In the OBE model [1], the long-range part of the NN interaction is attributed to one-pion exchange. The short-range part is described by ρ, ω-meson exchange or phenomenological repulsive core, while the σ-meson exchange is responsible for the intermediate-range attraction. Phenomenological form factors are needed to achieve the quantitative description of the NN interaction data. In the chiral perturbation theory [2], the multi-π's are exchanged between two nucleons. The short-range part related to the nucleon internal structure is modeled by the contact terms with phenomenological low-energy constants. The theory can give a quantitative description of the low-energy NN scattering below the π production threshold. It is hard to extend this model to higher energy, the very interesting resonance region of NN scattering.

With the advent of quantum chromodynamics (QCD), it is expected to describe the NN interaction from the fundamental degree of freedom of QCD, quark, and gluon. Recently, lattice QCD calculation has achieved a qualitative description of NN interaction [4]. However, it is still far from the quantitative description. The QCD-inspired quark models are useful in describing the NN interaction with the fundamental quark-gluon degree of freedom. The most popular and successful one is the constituent quark model. The nonperturbative (color confinement and spontaneous chiral symmetry breaking) and perturbative properties of QCD are incorporated into the model by introducing the phenomenological confinement potential, Goldstone-boson exchange, and effective one-gluon exchange between the massive constituent quarks [5]. In almost all realistic quark models aimed to describe the NN interaction, the short-range repulsion of NN interaction is described by one-gluon exchange and quark antisymmetrization. The long-range part is described by π-meson exchange, which is the same as the OBE and chiral perturbation theory approaches. To describe the intermediate-range part, the σ-meson exchange

is employed in most quark-model approaches. The only one exception is the quark delocalization color screening model (QDCSM). The quark delocalization and color screening effect between interacting quarks within different quark clusters are employed [6] to describe the intermediate-range attraction, which is similar to the molecular covalent bond. To develop such a molecular covalent-bond-like model, the outstanding fact is that the molecular force and nuclear force are similar except for the energy and length scale difference [7]. Also, the existence of the σ meson is not sure for long. Recently, BES collaboration reported the observation of the σ meson, which appeared as a $\pi\pi$ S-wave resonance [8]. However, the calculation of the correlated $\pi\pi$ exchange between two nucleons can not obtain enough attraction [9] as the phenomenological σ-meson exchange did. The recent QDCSM calculation, on the other hand, showed that the quark delocalization and color screening mechanism is quantitatively equivalent to the phenomenological σ-meson exchange in describing the NN intermediate-range attraction [10]. In ChPT, there is also no σ-meson exchange. In addition, by introducing the multibody color confinement interaction [11], or by incorporating the hidden color channels in the calculation [12], the intermediate-range attraction can also be obtained to some extent. Therefore, the mechanism of the NN intermediate-range attraction is still an open question.

In this work, an alternative approach for the NN interaction is studied. The hidden color channels ignored in the prevailing quark-model calculations of the NN interaction are included. Accordingly, the confinement potential between different channels is modified as follows: the ordinary confinement is used for the quark pairs within the same nucleon and the color singlet channels, whereas a multiplying factor is introduced for the confinement potential between the quark pairs if a hidden color channel is involved. The aim is to test if the color screening phenomenology used in QDCSM is an effective description of the hidden color channel coupling. The details of this model approach will be explained in the next section. The NN scattering phase shifts obtained in this approach are confronted with experimental data and compared with chiral quark model (ChQM) and QDCSM approaches. The

equivalence of these three quark models in describing the NN scattering data has been confirmed. The deuteron properties and dibaryon candidates are also studied with this model.

The structure of this paper is as follows. A brief introduction of the three quark models used is given in Sec. II. Section III is devoted to the numerical results and discussions. The summary is shown in the last section.

II. THREE QUARK MODELS

A. Chiral quark model

The Salamanca version of ChQM is chosen as the representative of the chiral quark models. It has been successfully applied to hadron spectroscopy and NN interaction. The model details can be found in Ref. [13]. Only the Hamiltonian and parameters are given here. The ChQM Hamiltonian in the nucleon-nucleon sector is

$$H = \sum_{i=1}^{6} \left(m_i + \frac{p_i^2}{2m_i} \right) - T_c + \sum_{i<j} [V^G(r_{ij}) + V^\pi(r_{ij}) + V^\sigma(r_{ij}) + V^C(r_{ij})],$$

$$V^G(r_{ij}) = \frac{1}{4}\alpha_s \lambda_i \cdot \lambda_j \left[\frac{1}{r_{ij}} - \frac{\pi}{m_q^2} \left(1 + \frac{2}{3}\sigma_i \cdot \sigma_j \right) \delta(r_{ij}) - \frac{3}{4m_q^2 r_{ij}^3} S_{ij} \right] + V_{ij}^{G,LS},$$

$$V_{ij}^{G,LS} = -\frac{\alpha_s}{4}\lambda_i \cdot \lambda_j \frac{1}{8m_q^2} \frac{3}{r_{ij}^3} [\mathbf{r}_{ij} \times (\mathbf{p}_i - \mathbf{p}_j)] \cdot (\sigma_i + \sigma_j),$$

$$V^\pi(r_{ij}) = \frac{1}{3}\alpha_{ch} \frac{\Lambda^2}{\Lambda^2 - m_\pi^2} m_\pi \left\{ \left[Y(m_\pi r_{ij}) - \frac{\Lambda^3}{m_\pi^3} Y(\Lambda r_{ij}) \right] \sigma_i \cdot \sigma_j + \left[H(m_\pi r_{ij}) - \frac{\Lambda^3}{m_\pi^3} H(\Lambda r_{ij}) \right] S_{ij} \right\} \tau_i \cdot \tau_j, \qquad (1)$$

$$V^\sigma(r_{ij}) = -\alpha_{ch} \frac{4m_u^2}{m_\pi^2} \frac{\Lambda^2}{\Lambda^2 - m_\sigma^2} m_\sigma \left[Y(m_\sigma r_{ij}) - \frac{\Lambda}{m_\sigma} Y(\Lambda r_{ij}) \right] + V_{ij}^{\sigma,LS}, \quad \alpha_{ch} = \frac{g_{ch}^2}{4\pi} \frac{m_\pi^2}{4m_u^2}$$

$$V_{ij}^{\sigma,LS} = -\frac{\alpha_{ch}}{2m_\pi^2} \frac{\Lambda^2}{\Lambda^2 - m_\sigma^2} m_\sigma^3 \left[G(m_\sigma r_{ij}) - \frac{\Lambda^3}{m_\sigma^3} G(\Lambda r_{ij}) \right] [\mathbf{r}_{ij} \times (\mathbf{p}_i - \mathbf{p}_j)] \cdot (\sigma_i + \sigma_j),$$

$$V^C(r_{ij}) = -a_c \lambda_i \cdot \lambda_j \left(r_{ij}^2 + V_0 \right) + V_{ij}^{C,LS},$$

$$V_{ij}^{C,LS} = -a_c \lambda_i \cdot \lambda_j \frac{1}{8m_q^2} \frac{1}{r_{ij}} \frac{dV^c}{dr_{ij}} [\mathbf{r}_{ij} \times (\mathbf{p}_i - \mathbf{p}_j)] \cdot (\sigma_i + \sigma_j), \quad V^c = r_{ij}^2$$

$$S_{ij} = \frac{(\sigma_i \cdot \mathbf{r}_{ij})(\sigma_j \cdot \mathbf{r}_{ij})}{r_{ij}^2} - \frac{1}{3}\sigma_i \cdot \sigma_j,$$

where S_{ij} is quark tensor operator, $Y(x)$, $H(x)$, and $G(x)$ are standard Yukawa functions [3], T_c is the kinetic energy of the center of mass, and α_{ch} is the chiral coupling constant, determined as usual from the π-nucleon coupling constant. All other symbols have their usual meanings. The parameters of this ChQM Hamiltonian are given in Table I.

TABLE I. Parameters of three-quark models discussed in this paper.

	ChQM	QDCSM1	QDCSM2	QDCCM
$m_{u,d}$ (MeV)	313	313	313	313
b (fm)	0.518	0.518	0.60	0.518
a_c (MeV fm^{-2})	46.938	56.755	18.5	56.755
V_0 (fm^2)	−1.297	−0.5279	−1.3598	−0.5279
μ (fm^{-2})		0.45	1.00	
α_s	0.485	0.485	0.996	0.485
m_π (MeV)	138	138	138	138
α_{ch}	0.027	0.027	0.027	0.027
m_σ (MeV)	675			
Λ (fm^{-1})	4.2	4.2	4.2	4.2

B. Quark delocalization color screening model

The model and its extension were discussed in detail in Refs. [14,15]. Its Hamiltonian has the same form as Eq. (1), but without σ-meson exchange, and a phenomenological color screening confinement potential is used:

$$V^C(r_{ij}) = -a_c \lambda_i \cdot \lambda_j [f(r_{ij}) + V_0] + V_{ij}^{C,LS},$$

$$f(r_{ij}) = \begin{cases} r_{ij}^2 & \text{if } i, j \text{ occur in the same} \\ & \text{baryon orbit,} \\ \frac{1-e^{-\mu r_{ij}^2}}{\mu} & \text{if } i, j \text{ occur in different} \\ & \text{baryon orbits.} \end{cases} \qquad (2)$$

Here, μ is the color screening constant to be determined by fitting the deuteron mass in this model. The quark delocalization in QDCSM is realized by allowing the single-particle orbital wave function of QDCSM as a linear combination of left and right Gaussian, the single-particle orbital wave functions in the ordinary quark cluster model:

$$\psi_\alpha(\vec{S}_i, \epsilon) = [\phi_\alpha(\vec{S}_i) + \epsilon\phi_\alpha(-\vec{S}_i)]/N(\epsilon),$$
$$\psi_\beta(-\vec{S}_i, \epsilon) = [\phi_\beta(-\vec{S}_i) + \epsilon\phi_\beta(\vec{S}_i)]/N(\epsilon),$$

TABLE II. The channels used in NN scattering calculations and the factors k_1, k_2 (for recipes 1,2) for each channel ($I = 1$).

J	Channels	k_1/k_2
0	$^1S_0 : NN, \Delta\Delta, {}^2\Delta_8^2\Delta_8, {}^4N_8^4N_8, {}^2N_8^2\Delta_8,$ $^2N_8^2N_8$	1.42/1.39
	$^5D_0 : N\Delta, \Delta\Delta, {}^4N_8^2\Delta_8, {}^4N_8^4N_8, {}^4N_8^2\Delta_8$	
	$^3P_0 : NN, N\Delta, \Delta\Delta, {}^2\Delta_8^2\Delta_8, {}^4N_8^2\Delta_8,$ ${}^4N_8^4N_8, {}^4N_8^2N_8, {}^2N_8^2\Delta_8, {}^2N_8^2N_8$	1.10/1.10
1	$^3P_1 : NN, N\Delta, \Delta\Delta, {}^2\Delta_8^2\Delta_8, {}^4N_8^2\Delta_8,$ ${}^4N_8^4N_8, {}^4N_8^2N_8, {}^2N_8^2\Delta_8, {}^2N_8^2N_8$	1.35/1.28
2	$^1D_2 : NN, \Delta\Delta, {}^2\Delta_8^2\Delta_8, {}^4N_8^4N_8, {}^2N_8^2\Delta_8,$ ${}^2N_8^2N_8$	2.00/1.85
	$^5S_2({}^5D_2) : N\Delta, \Delta\Delta, {}^4N_8^2\Delta_8, {}^4N_8^4N_8,$ ${}^4N_8^2\Delta_8$	
	$^3P_2 : NN, N\Delta, \Delta\Delta, {}^2\Delta_8^2\Delta_8, {}^4N_8^2\Delta_8,$ ${}^4N_8^4N_8, {}^4N_8^2N_8, {}^2N_8^2\Delta_8, {}^2N_8^2N_8$	1.75/1.66
	$^3F_2 : NN, N\Delta, \Delta\Delta, {}^2\Delta_8^2\Delta_8, {}^4N_8^2\Delta_8,$ ${}^4N_8^4N_8, {}^4N_8^2N_8, {}^2N_8^2\Delta_8, {}^2N_8^2N_8$	1.00/1.00
3	$^3F_3 : NN, N\Delta, \Delta\Delta, {}^2\Delta_8^2\Delta_8, {}^4N_8^2\Delta_8,$ ${}^4N_8^4N_8, {}^4N_8^2N_8, {}^2N_8^2\Delta_8, {}^2N_8^2N_8$	1.00/1.00
4	$^3F_4 : NN, N\Delta, \Delta\Delta, {}^2\Delta_8^2\Delta_8, {}^4N_8^2\Delta_8,$ ${}^4N_8^4N_8, {}^4N_8^2N_8, {}^2N_8^2\Delta_8, {}^2N_8^2N_8$	1.00/1.00
	$^1G_4 : NN, \Delta\Delta, {}^2\Delta_8^2\Delta_8, {}^4N_8^4N_8, {}^2N_8^2\Delta_8,$ ${}^2N_8^2N_8$	1.00/1.00
	$^3H_4 : NN, N\Delta, \Delta\Delta, {}^2\Delta_8^2\Delta_8, {}^4N_8^2\Delta_8,$ ${}^4N_8^4N_8, {}^4N_8^2N_8, {}^2N_8^2\Delta_8, {}^2N_8^2N_8$	1.00/1.00
5	$^3H_5 : NN, N\Delta, \Delta\Delta, {}^2\Delta_8^2\Delta_8, {}^4N_8^2\Delta_8,$ ${}^4N_8^4N_8, {}^4N_8^2N_8, {}^2N_8^2\Delta_8, {}^2N_8^2N_8$	1.00/1.00
6	$^3H_6 : NN, N\Delta, \Delta\Delta, {}^2\Delta_8^2\Delta_8, {}^4N_8^2\Delta_8,$ ${}^4N_8^4N_8, {}^4N_8^2N_8, {}^2N_8^2\Delta_8, {}^2N_8^2N_8$	1.00/1.00
	$^1I_6 : NN, \Delta\Delta, {}^2\Delta_8^2\Delta_8, {}^4N_8^4N_8, {}^2N_8^2\Delta_8,$ ${}^2N_8^2N_8$	1.00/1.00

TABLE III. The channels used in NN scattering calculations and the factors k_1, k_2 (for recipes 1,2) for each channel ($I = 0$).

J	Channels	k_1/k_2
1	$^3S_1({}^3D_1) : NN, \Delta\Delta, {}^2\Delta_8^2\Delta_8, {}^4N_8^4N_8,$ ${}^4N_8^2N_8, {}^2N_8^2N_8$	1.40/1.38
	$^7D_1 : \Delta\Delta, {}^4N_8^4N_8$	
	$^1P_1 : NN, \Delta\Delta, {}^2\Delta_8^2\Delta_8, {}^4N_8^4N_8, {}^2N_8^2N_8$	1.80/1.70
	$^5P_1 : \Delta\Delta, {}^4N_8^4N_8, {}^4N_8^2N_8$	
2	$^3D_2 : NN, \Delta\Delta, {}^2\Delta_8^2\Delta_8, {}^4N_8^4N_8, {}^4N_8^2N_8,$ ${}^2N_8^2N_8$	1.00/1.00
	$^7D_2 : \Delta\Delta, {}^4N_8^4N_8$	
3	$^3D_3 : NN, \Delta\Delta, {}^2\Delta_8^2\Delta_8, {}^4N_8^4N_8, {}^4N_8^2N_8,$ ${}^2N_8^2N_8$	2.40/2.20
	$^7S_3({}^7D_3) : \Delta\Delta, {}^4N_8^4N_8$	
	$^1F_3 : NN, \Delta\Delta, {}^2\Delta_8^2\Delta_8, {}^4N_8^4N_8,$ ${}^2N_8^2N_8$	1.00/1.00
	$^3G_3 : NN, \Delta\Delta, {}^2\Delta_8^2\Delta_8, {}^4N_8^4N_8,$ ${}^4N_8^2N_8, {}^2N_8^2N_8$	1.00/1.00
4	$^3G_4 : NN, \Delta\Delta, {}^2\Delta_8^2\Delta_8, {}^4N_8^4N_8, {}^4N_8^2N_8,$ ${}^2N_8^2N_8$	1.00/1.00
5	$^3G_5 : NN, \Delta\Delta, {}^2\Delta_8^2\Delta_8, {}^4N_8^4N_8, {}^4N_8^2N_8,$ ${}^2N_8^2N_8$	1.00/1.00
	$^1H_5 : NN, \Delta\Delta, {}^2\Delta_8^2\Delta_8, {}^4N_8^4N_8,$ ${}^2N_8^2N_8$	1.00/1.00
	$^3I_5 : NN, \Delta\Delta, {}^2\Delta_8^2\Delta_8, {}^4N_8^4N_8, {}^4N_8^2N_8,$ ${}^2N_8^2N_8$	1.00/1.00
6	$^3I_6 : NN, \Delta\Delta, {}^2\Delta_8^2\Delta_8, {}^4N_8^4N_8, {}^4N_8^2N_8,$ ${}^2N_8^2N_8$	1.00/1.00
7	$^3I_7 : NN, \Delta\Delta, {}^2\Delta_8^2\Delta_8, {}^4N_8^4N_8, {}^4N_8^2N_8,$ ${}^2N_8^2N_8$	1.00/1.00

$$N(\epsilon) = \sqrt{1 + \epsilon^2 + 2\epsilon e^{-S_i^2/4b^2}},$$

$$\phi_\alpha(\vec{S}_i) = \left(\frac{1}{\pi b^2}\right)^{3/4} e^{-\frac{1}{2b^2}(\vec{r}_\alpha - \vec{S}_i/2)^2},$$

$$\phi_\beta(-\vec{S}_i) = \left(\frac{1}{\pi b^2}\right)^{3/4} e^{-\frac{1}{2b^2}(\vec{r}_\beta + \vec{S}_i/2)^2}. \tag{3}$$

The mixing parameter $\epsilon(S)$ is not an adjusted one but is determined variationally by the dynamics of the multiquark system itself. This assumption allows the multiquark system to choose its favorable configuration in the interacting process. It has been used to explain the crossover transition between the hadron phase and the quark-gluon plasma phase [16]. The model parameters are fixed as follows: The u, d-quark mass difference is neglected and $m_u = m_d$ is assumed to be exactly 1/3 of the nucleon mass, namely, $m_u = m_d = 313$ MeV. The π mass takes the experimental value. The Λ takes the same values as in Ref. [3], namely, $\Lambda = 4.2$ fm^{-1}. The chiral coupling constant α_{ch} is determined from the πNN coupling constant as usual. The other parameters b, a_c, V_0, and α_s are determined by fitting the nucleon and Δ masses and the stability of nucleon size b with the variation of quark mass m. All parameters used are listed in Table I. In order to compare the intermediate-range

attraction mechanism, the σ-meson exchange in ChQM, and quark delocalization and color screening in QDCSM, the same values of parameters b, α_s, α_{ch}, m_u, m_π, Λ are used for these two models. Thus, these two models have exactly the same contributions from one-gluon exchange and π exchange. The only difference of the two models is coming from the short- and intermediate-range parts, σ exchange for ChQM, quark delocalization, and color screening for QDCSM. To show the sensitivity of the QDCSM to the model parameters, the results of another set of model parameters (QDCSM2) is also reported.

C. Quark delocalization model with hidden color channels coupling (QDCCM)

This approach is focused on the hidden color channel effect, which has been ignored almost in all quark-model calculations, but certainly should exist in a description based on the fundamental quark-gluon degree of freedom. In the lattice QCD calculation of the NN interaction [4], these hidden color channels should have been included implicitly. However, their effect has not yet been separated. We assume a Hamiltonian that is the same as that of QDCSM, except that the usual quadratic confinement

$$V^C(r_{ij}) = -k a_c \lambda_i \cdot \lambda_j \left(r_{ij}^2 + V_0\right) \tag{4}$$
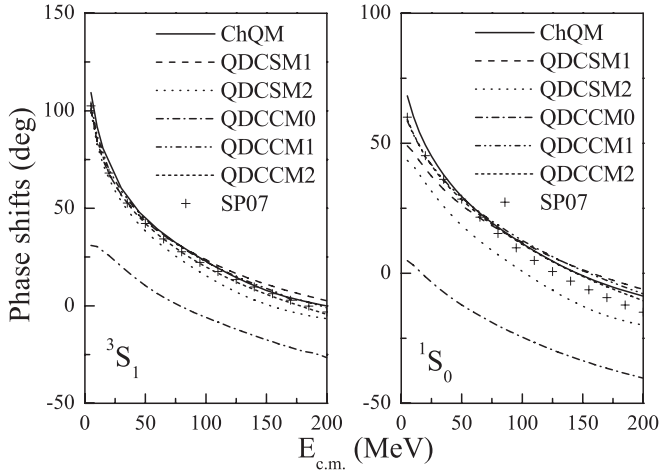
FIG. 1. The phase shifts of NN S-wave scattering.

is used, but with an additional multiplying factor k. For the color singlet channels (two baryon clusters are in the color singlet states), the factor k takes the value 1. For the hidden color channels, two recipes are used. Recipe 1 (QDCCM1): For the coupling between hidden color channels and the color singlet channels, the factor k is taken as an adjustable

parameter. In all the other cases, the factor k is kept 1. Recipe 2 (QDCCM2): The factor k is taken as an adjustable parameter not only for color singlet–hidden color channels coupling, but also for hidden color–hidden color channels. As for the single-quark orbital wave function, the same form [Eq. (3)] as that of QDCSM is assumed. This model assumption is inspired by the lattice QCD calculation: The recent lattice QCD calculations show that the interactions among quarks are genuinely multibody interactions. The color-dependent two-body confinement interaction is consistent with the lattice QCD results only for two- and three-quark systems in color singlet states, but inconsistent with the multibody interaction obtained in lattice QCD for multiquark systems [17]. So, the direct extension of the color-dependent two-body confinement interaction from the two- or three-quark system to the multiquark system as used in most quark-model calculations is questionable. The calculation based on the direct extension can not describe the NN scattering quantitatively well, even after including hidden color channels coupling as shown in QDCCM0, which might be an indication of this inadequacy. In fact, for multiquark systems and color octet nucleons, quark pairs are not always in color-antisymmetric states, but also in color-symmetric ones. The color factor $\boldsymbol{\lambda}_i \cdot \boldsymbol{\lambda}_j$ will give rise to anticonfinement interaction for symmetric quark pairs [18]. In QDCSM mentioned above, we used a color screening
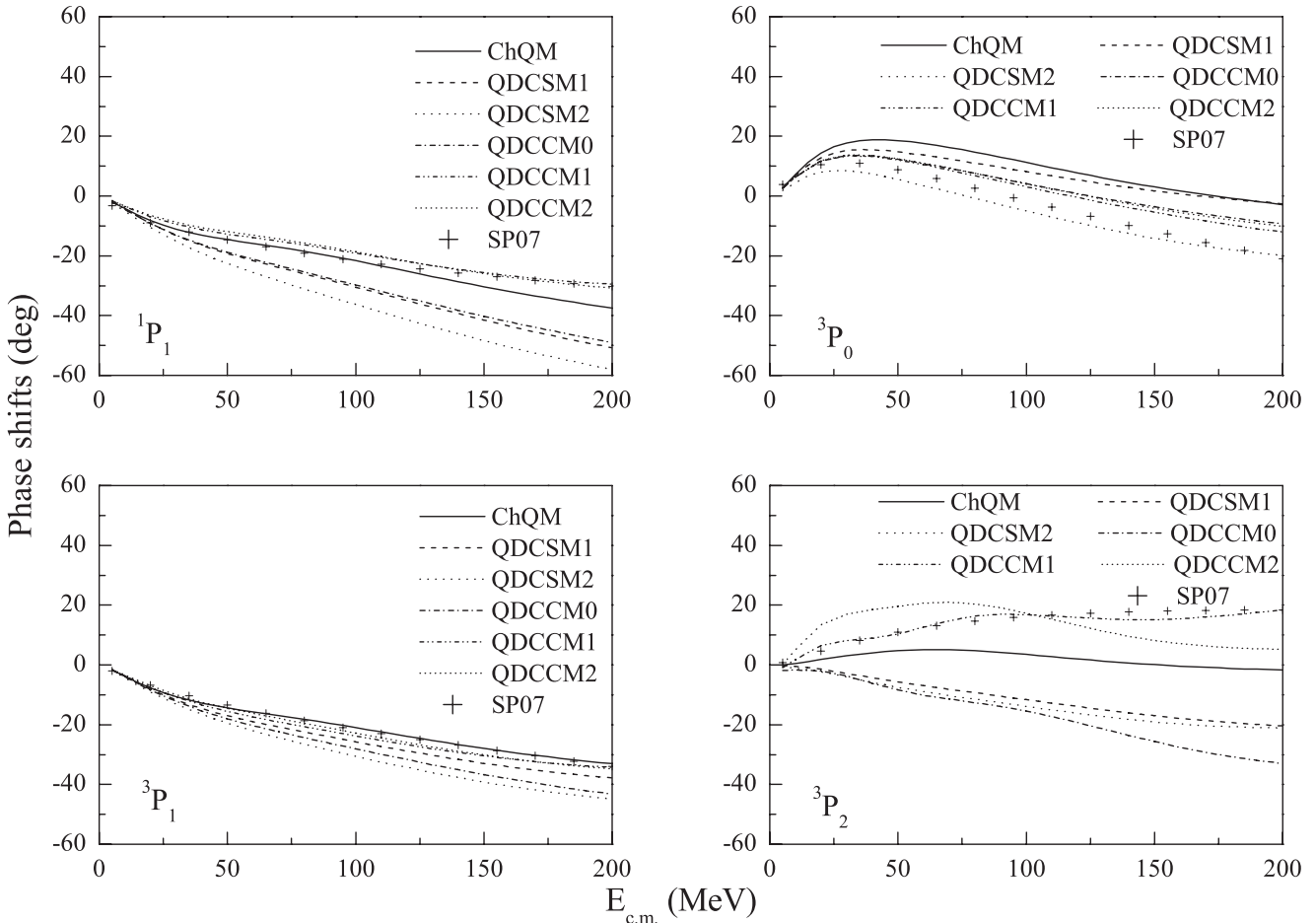
FIG. 2. The phase shifts of NN P wave scattering.
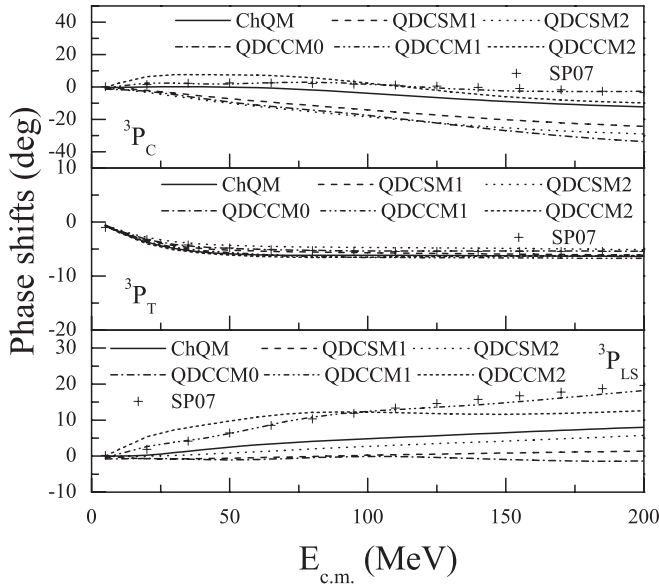
FIG. 3. Central, spin-orbit, and tensor components of NN P-wave scattering.

confinement interaction to model the effect of this multibody confinement interaction obtained in lattice QCD. Here, we

study directly the effect of hidden color channel coupling to test if the phenomenological color screening confinement is an effective description of the hidden channel coupling. In order to simplify the numerical calculation, a two-body confinement interaction form [Eq. (4)] is still assumed, but with an additional adjustable multiplying factor aimed to reflect the effect of the lattice QCD multibody confinement. At the same time, the model parameters are kept to the same as those of QDCSM1, except the color screening confinement form [Eq. (2)] is replaced by the usual quadratic confinement form [Eq. (4)]. This is aimed to let the effect of hidden color channel coupling stand out.

III. THE RESULTS AND DISCUSSIONS

We calculated the NN scattering phase shifts of different partial waves (S, P, D, F, G, H, and I waves) by the three-quark models mentioned above. To look for nonstrange dibaryon resonances, a systematic calculation of NN scattering phase shifts with explicit coupling to $N\Delta$ and $\Delta\Delta$ channels is also done. The resonating-group method (RGM), described in more detail in Ref. [19], is used to do the calculation. The experimental information used for the comparison is the partial-wave solution SP07 [20] of NN scattering data. For QDCSM, the color screening parameter μ is fixed by deuteron properties, and no other parameters are readjusted. For the third
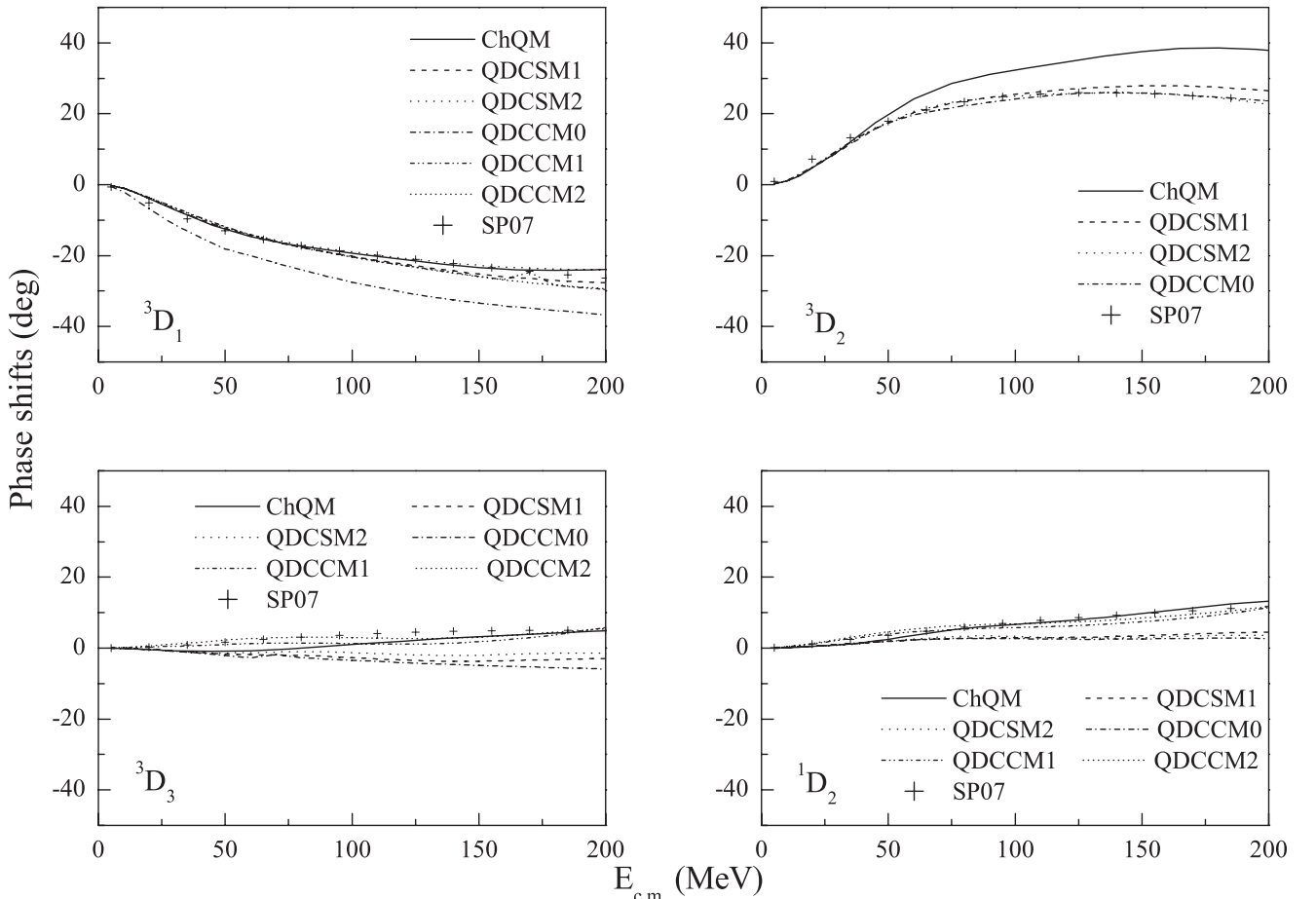
FIG. 4. The phase shifts of NN D-wave scattering.
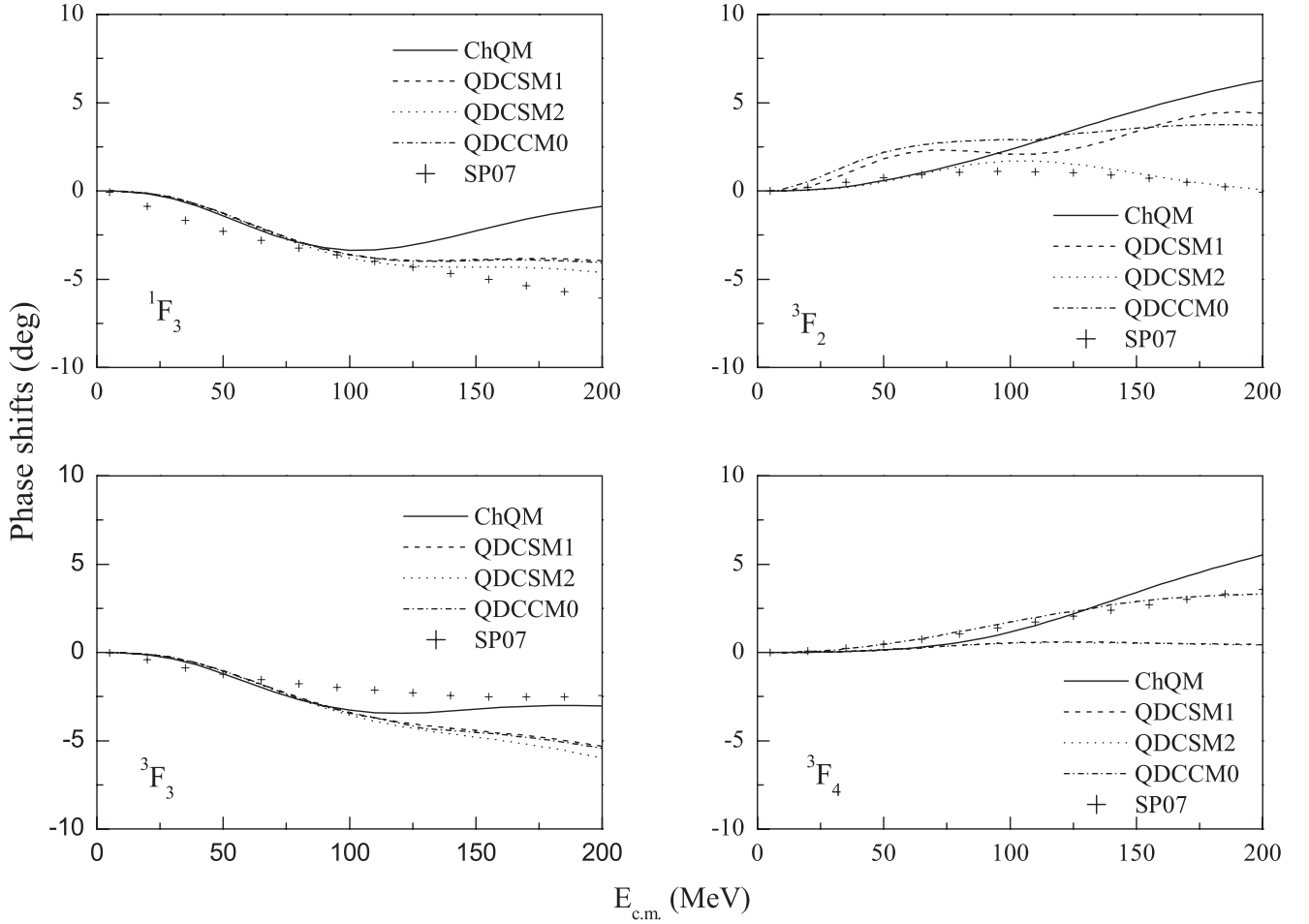
FIG. 5. The phase shifts of NN F-wave scattering.

approach (QDCCM), the channels included in different partial waves are listed in Tables II and III. The multiplying factors k_1, k_2 are adjusted to fit the NN phase shifts of SP07. The calculated results for NN scattering phase shifts are presented in Sec. III A; deuteron properties are shown in Sec. III B and the discussions of the dibaryon resonances are given in Sec. III C.

A. NN scattering phase shifts

(1) S waves: Figure 1 shows the NN scattering phase shifts for $^3S_1$ and $^1S_0$ partial waves. A perfect fit is obtained for both ChQM and QDCSM1 (QDCSM2 gives a little less attraction). The dominant contribution to the S-wave phase shift comes from the central part of the potentials. The agreement between two models means these two quark models give the same NN interaction, at least the same central part. For QDCCM, QDCCM1 and QDCCM2 also give good descriptions of NN $^3S_1$ and $^1S_0$ scattering phase shifts by including the hidden color channels and adjusting the color confinement interaction strength, while with the usual color confinement interaction strength ($k = 1$), the model (QDCCM0) calculated phase shifts are far from the measured ones.

(2) P waves: Figure 2 shows the NN scattering phase shifts of $^1P_1$, $^3P_0$, $^3P_1$, and $^3P_1$ partial waves. For $^1P_1$ and $^3P_1$, ChQM and QDCCM gave an almost perfect description of the experimental data. The $^1P_1$ phase shift is mainly determined by the central repulsion. The theoretical phase shifts of QDCSM and QDCCM0 are lower than experimental ones, which show that these two models give a too strong repulsion. For $^3P_0$, QDCSM2 described the experimental data better than others. For QDCCM, we do not have to adjust the color confinement interaction strength a_c too much ($k = 1.1$ for both QDCCM1 and QDCCM2), so both QDCCM1 and QDCCM2, even QDCCM0, can fit the $^3P_0$ phase shifts reasonably well. ChQM and QDCSM1 give too strong attraction. For $^3P_2$, QDCSM1 gives a perfect fit. ChQM, QDCSM, and QDCCM0 do not have enough attraction. Figure 3 shows central, spin-orbit, and tensor components of the ^3P_J phase shifts. Clearly, ChQM, QDCSM, and QDCCM0 do not give strong enough attraction in the central and spin-orbit parts. In OBE, $\pi\rho$ and $\pi\omega$ exchange, which might not have been reproduced in the quark-model calculations, are also needed to reproduce the P-wave phase shifts [1].

(3) D waves: Figure 4 shows the NN scattering phase shifts of $^3D_1$, $^3D_2$, $^3D_3$, and $^1D_2$ partial waves. For $^3D_1$, all the models fit the experimental data well except QDCCM0. For
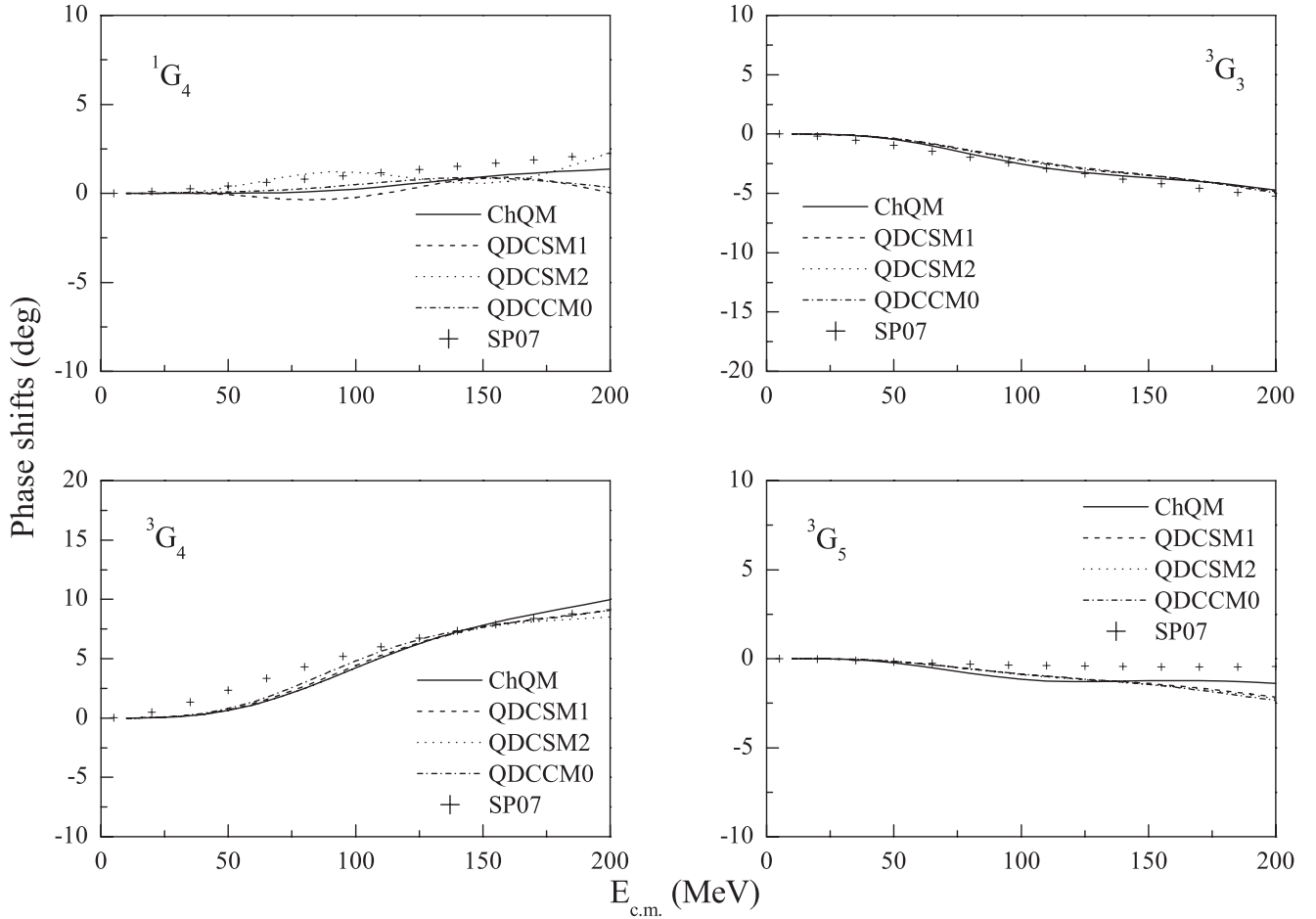
FIG. 6. The phase shifts of NN G-wave scattering.

$^3D_2$, QDCSM1 and QDCSM2 give a very good description of the experimental data (QDCSM2 is a little better), and ChQM gives too strong attraction. For QDCCM, we find that we do not need to adjust the color confinement interaction strength for this channel, and QDCCM0 can fit the experimental scattering phase shifts. For $^3D_3$ and $^1D_2$, ChQM described the experimental data better than QDCSM. For QDCCM, both adjusting recipes can give a perfect fit to the experimental data.

(4) F wave: The calculated $^1F_3$, $^3F_2$, $^3F_3$, and $^3F_4$ NN phase shifts are shown in Fig. 5. For F-wave scattering, we find that QDCCM0 already fit the experimental scattering phase shifts reasonably, so we did not fine tune the confinement strength. All the models give a good description of the experimental data reasonably in the low-energy region ($E_{c.m.} < 100$ MeV). Above 100 MeV, the model predictions deviate more or less from the experimental data. For $^3F_2$, QDCSM2 gave a much better fit to the experimental data than QDCSM1, ChQM, and QDCCM0. For $^1F_3$, QDCSM1, QDCSM2, and QDCCM0 all give a better fit to the experimental data than ChQM, especially at higher energy. However, for $^3F_3$, ChQM is closer to the experimental data than other models. For $^3F_4$, a perfect fit is obtained for QDCCM0, ChQM has a little too strong attraction at high energy, and QDCSM gives a too weak attraction.

(5) G wave: The NN phase shifts of $^3G_3$, $^1G_4$, $^3G_4$, and $^3G_5$ are shown in Fig. 6. All the models can describe the experimental data. We do not have to adjust the color confinement interaction strength for QDCCM here.

(6) H wave: Figure 7 shows the calculated $^1H_5$, $^3H_4$, $^3H_5$, and $^3H_6$ NN phase shifts. For H-wave phase shifts, all models fit to the experimental data equally well. We also find that we do not have to adjust the color confinement interaction strength for QDCCM here.

(7) I wave: The calculated $^3I_5$, $^1I_6$, $^3I_6$, and $^3I_7$ NN phase shifts are shown in Fig. 8. For I-wave phase shifts, all the models give almost the same results and fit the experimental data well. Again, the color confinement interaction strength for QDCCM does not need to be adjusted here.

For high-L partial waves, the long-range π exchange dominates the interaction. Three quark models have the same π exchange and therefore give almost the same results for $L \geqslant 3$, and we do not have to adjust the multiplying factor for the QDCCM for these high-L partial waves.

These numerical results (Figs. 1–8) show that by including the hidden color channels and adjusting the color confinement interaction strength, both adjusting recipes can fit the NN scattering phase shifts well. From the calculated S-, P-, and
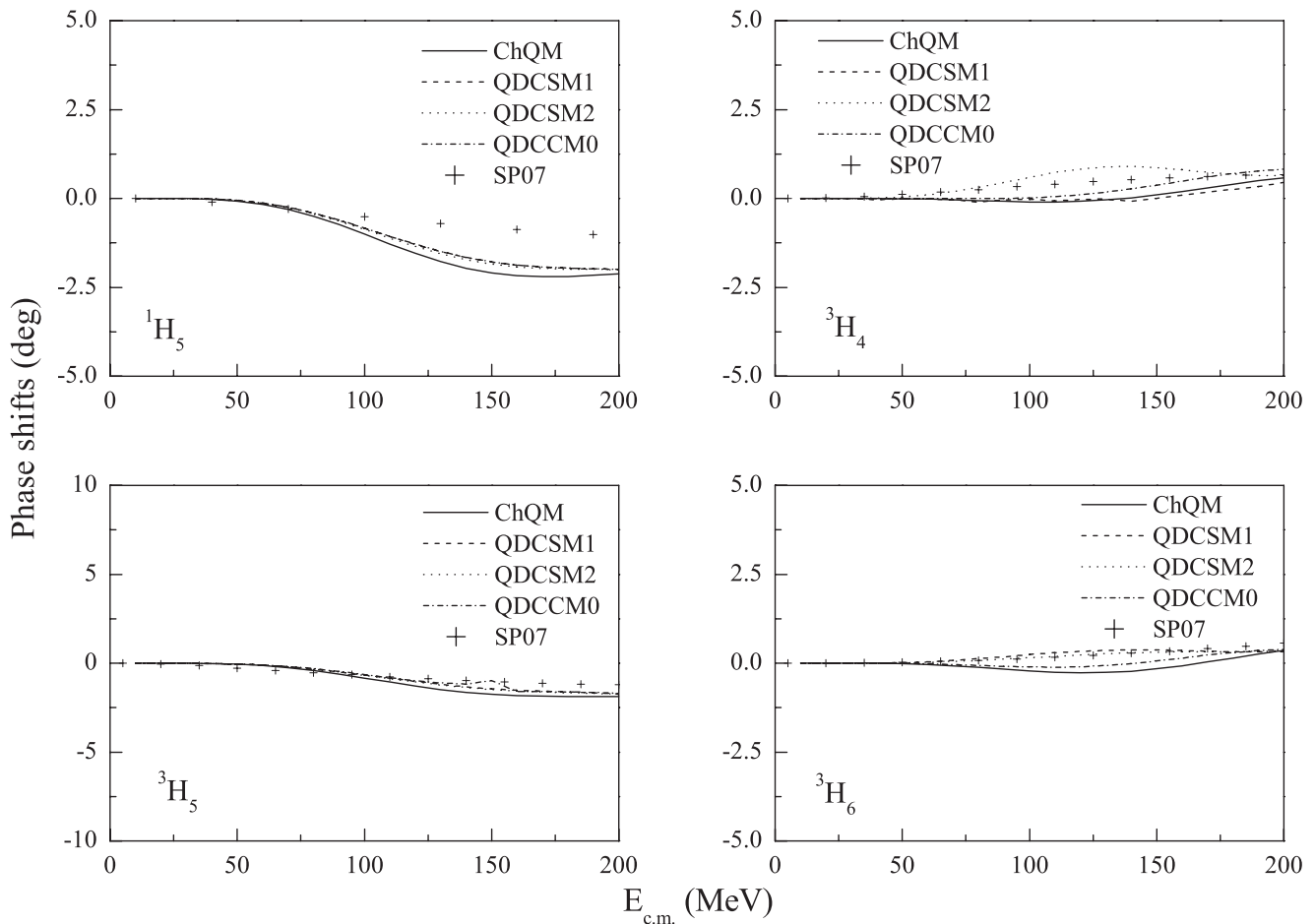
FIG. 7. The phase shifts of NN H-wave scattering.

D-wave phase shifts of NN scattering in QDCCM0, we can see that the attraction is always inadequate because of the appearance of anticonfinement interaction of symmetric quark pairs. By increasing the strength of confinement, the attraction coming from the confinement interaction is strengthened, and QDCCM1 and QDCCM2 can give a good description of the experimental data. We take these results as an indication that the short- and intermediate-range NN interaction is caused by the nucleon internal structure and its distortion both in orbital and color spaces in the interacting process. These are quite the same as the atomic internal structure and its distortion in orbital space, which gives rise to the molecular covalent bond. The Anderson's conjecture [7] is verified here. The phenomenological color screening confinement might be an effective description of the hidden color channel coupling. The phenomenological σ-meson exchange used in OBE and ChQM might be an effective description of the more complicated nucleon distortion in the NN interaction process as described in QDCSM and QDCCM. This mechanism also gives a natural explanation as to why the NN interaction between two color singlet nucleons is so similar to the molecular interaction between two charge neutral atoms, except for the energy and length scale difference.

B. Deuteron

All these three models are used to calculate the properties of deuteron, and the results are shown in Table IV. Both ChQM and QDCSM give a good description of deuteron. For QDCSM, by adjusting the color screening parameter, the same results for deuteron can be obtained for different baryon size b. Because of the large separation between the proton and neutron in the deuteron, the properties of deuteron mainly reflect the long-range part of the nuclear force. The same π exchange used in the two models assure that the properties of deuteron can be fitted equally well. However, π exchange alone can not provide strong enough intermediate-range attraction to make the deuteron bound. In ChQM, it is the phenomenological σ-meson exchange that provides the intermediate-range attraction. In QDCSM, it is the quark delocalization and color screening that provide the intermediate-range attraction. The fact that both models fit the deuteron properties well verifies once more that the two intermediate-range attraction mechanisms used in these two models are equivalent.

Table IV shows that the binding energy and the D-wave component of deuteron can be reproduced (we did not fine tune the strength of color confinement to get a better fitting). However, the root-mean-square radius is too small
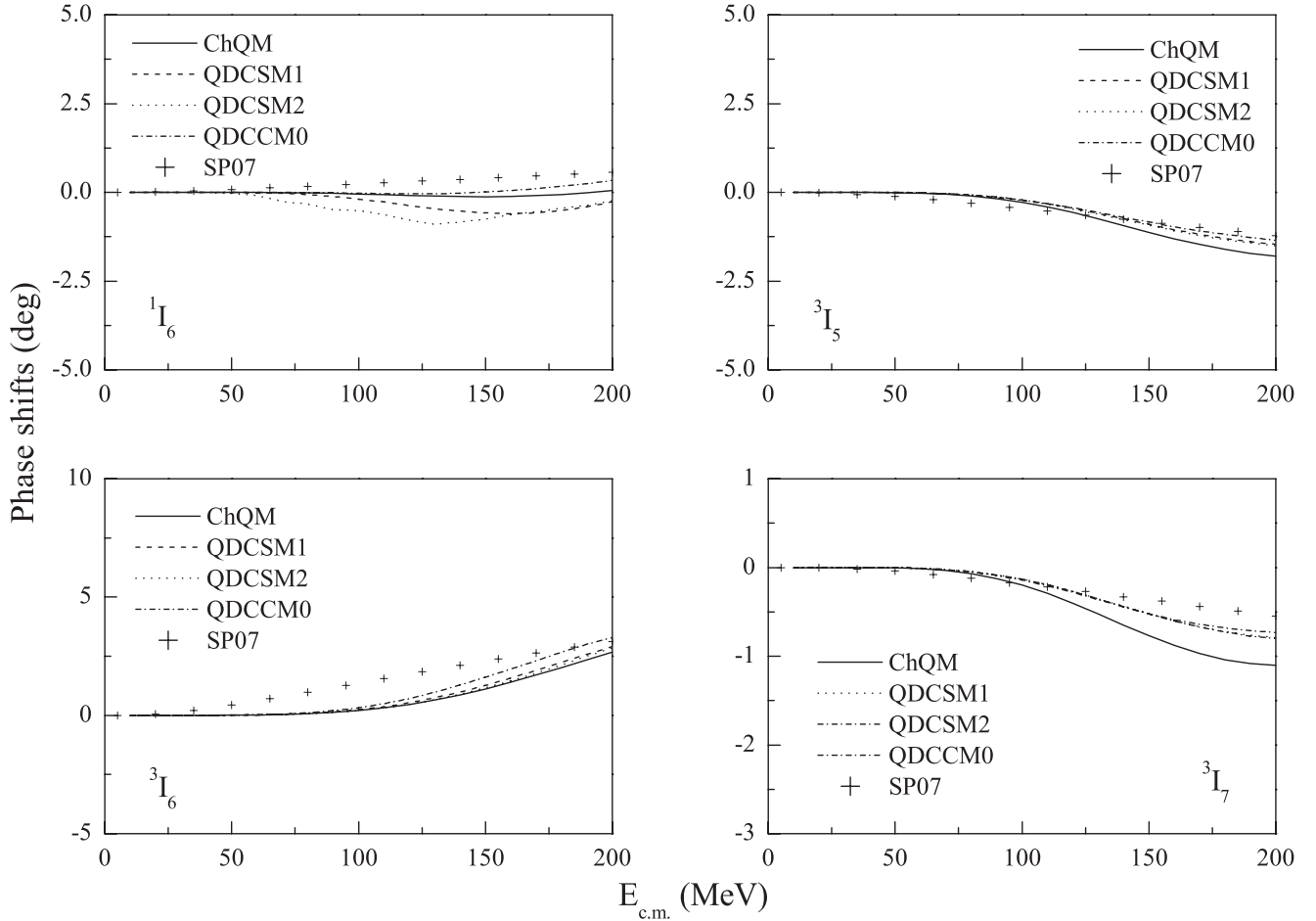
FIG. 8. The phase shifts of NN I-wave scattering.

in comparison to experimental value. This may indicate that QDCCM with the parameters given in Table I gives rise to an NN scattering phase shift equivalent potential, but with a little too strong attraction in the short-range region, which tightens up the deuteron.

C. Dibaryon resonances in NN scattering

In this section, we show the results of a systematic search for the possible nonstrange dibaryon candidates by the three-quark models mentioned above.

The previous calculations [21] show that there are four possible dibaryons in the quark-model calculations, $N\Delta$ state with $IJ = 12$, $\Delta\Delta$ states with $IJ = 01, 10, 03$. Here, the QDCCM is applied to recalculate these states. All of these dibaryon states are allowed to decay via the NN channels. In

other words, these dibaryon states appear as resonance states in the NN scattering process. So, we calculate the NN scattering phase shifts by including all the possible channel couplings. The results are shown in Fig. 9.

(1) $I = 0$, $J = 1$: The $^3S_1$ energies of single Δ-Δ channel calculation are lower than the corresponding threshold 100–350 MeV in ChQM, QDCCM, and QDCSM. The coupling to the $^3S_1^{NN}$ channel has an unexpectedly large effect, pushing up the energy of $^3S_1^{\Delta\text{-}\Delta}$ state ~ 300 MeV, so that only in QDCSM2 it becomes a resonance at 2408 MeV. This very large mass shift is caused by the central interaction and the presence of a lower-mass state, the deuteron, in the admixed $^3S_1^{NN}$ channel. Mixing with other channels listed in Table III, the resonance mass is pushed down a little bit, to 2393 MeV. In ChQM and QDCCM, the $^3S_1$ energies in the single Δ-Δ channel calculation are 100 MeV or more higher than that in QDCSM2. The additional large mass shift caused by the coupling to the NN channel then pushes the state above the $\Delta\Delta$ threshold. So, no resonance appears in other models except QDCSM2. The phase shifts of $^3S_1^{NN}$ are shown in the upper left corner of Fig. 9, where the phase shifts for $100 < E_{\text{c.m.}} < 400$ MeV from ChQM, QDCSM1, QDCSM2, QDCCM1, and QDCCM2 agree with each other, as already pointed out in Sec. III A. The phase

TABLE IV. The properties of deuteron.

	ChQM	QDCSM1	QDCSM2	QDCCM1	QDCCM2
B (MeV)	2.0	1.94	2.01	1.0	2.2
$\sqrt{r^2}$ (fm)	1.96	1.93	1.94	1.2	1.1
P_D (%)	4.86	5.25	5.25	4.0	4.0

shifts of $^3S_1^{NN}$ rise through $\pi/2$ at a resonance mass only in QDCSM2. So, whether there is an $IJ = 01$ $\Delta\Delta$ resonance state with resonance mass 2393 MeV in the NN $^3S_1$ scattering channel is unknown.

(2) $I = 0$, $J = 3$: The single Δ-Δ channel calculation shows that the state $^7S_3^{\Delta\Delta}$ is a bound state in all models used here. The coupling to the $^3D_3^{NN}$ channels causes this bound state to change into an elastic resonance. The resonance mass shift, which is caused by the tensor interaction, is not large (~ 3 MeV). The calculation shows that the mass shift is always dominated by the NN scattering states below the bound state rather than those above it. Coupling to other channels listed in Table III, which are above the $^7S_3^{\Delta\Delta}$ bound state, the resonance is pushed down as expected. The calculated $^3D_3^{NN}$ phase shifts, shown in the upper right corner of Fig. 9, rise through $\pi/2$ at the resonance masses in all models. But, quantitatively, the resonance masses are different in different models. The resonance mass in QDCSM1 is about 60 MeV lower than that in ChQM, and the QDCSM2 always has the lowest mass. For QDCCM, the resonance mass is 2443 MeV in QDCCM0, 2298 MeV in QDCCM1, and 2156 MeV in QDCCM2. This resonance ($IJ = 03$ $\Delta\Delta$) is a promising candidate for the observed isoscalar ABC structure seen more clearly in the $pn \rightarrow d\pi\pi$ production cross section

at 2.36 Gev in the recent report by the CELSIUS-WASA Collaboration [22].

(3) $I = 1$, $J = 0$: The $^1S_0^{\Delta\Delta}$ state is qualitatively similar to the $^3S_1^{\Delta\Delta}$ state since they are just different spin-isospin states of the same quark system with the same relative orbital angular momenta. The calculated phase shifts, shown in the lower left corner of Fig. 9, show that the resonance survives only in QDCSM2 after the channel coupling. The situation is almost the same as the $^3S_1^{NN}$ state.

(4) $I = 1$, $J = 2$: The phase shifts of NN scattering are shown in the lower right corner of Fig. 9. From the curves, we find that a resonance appears in QDCSM2, QDCCM1, and QDCCM2. The resonance masses are 2168 MeV in QDCSM2, 2144 MeV in QDCCM1, and 2130 MeV in QDCCM2. For ChQM and QDCSM1, only a prominent cusp appears at the $N\Delta$ threshold. Nevertheless, the state might correspond to the resonance looping in the Argand diagram of the $^1D_2$ pp partial wave [23].

For odd-parity NN states, resonance poles are found for the isovector odd-parity NN partial waves $^3P_2$, $^3F_2$, and $^3F_3$ [24]. These empirical resonancelike solutions reproduce the empirical Argand loopings of the partial-wave solutions, but many studies in the past [25] have not resolved the question of whether these Argand loopings represent real dibaryon
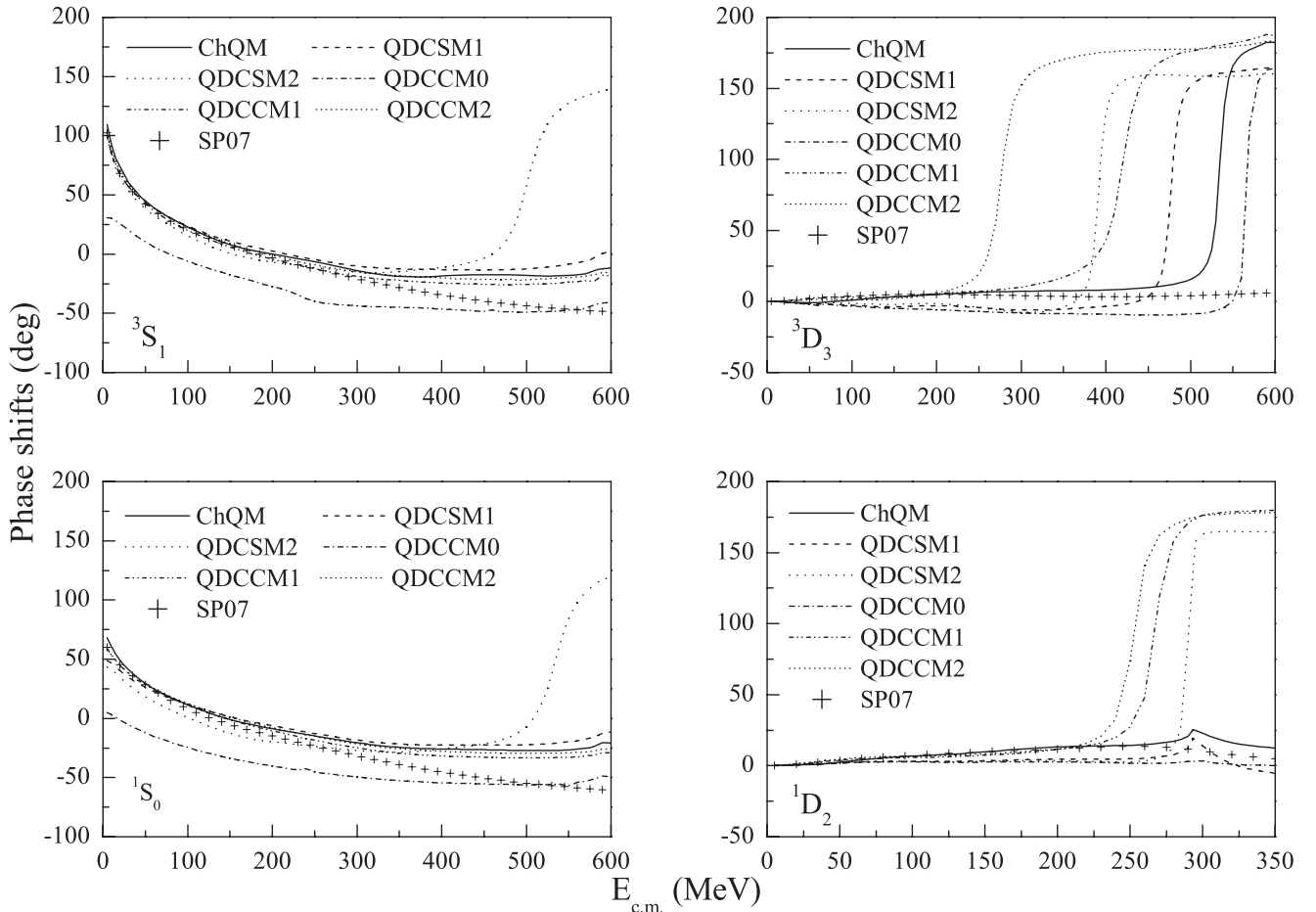
FIG. 9. The phase shifts of NN S-wave and D-wave scattering to energies beyond the $\Delta\Delta$ or $N\Delta$ thresholds.

resonances. In our quark-model calculation, we have not found any resonance attributable to an $N\Delta$ or $\Delta\Delta$ bound state in the odd-parity NN states.

IV. SUMMARY

By including the hidden color channels and varying the strength of the color confinement potential between color singlet channels and hidden color channels and/or hidden color channels and hidden color channels, a phenomenological quark model for baryon-baryon interaction is constructed. The model achieves a good description of S-, P-, D-, F-, G-, H-, and I-partial-wave phase shifts of NN scattering as good as other quark models. It also reproduces the binding energy and D-wave component of deuteron, but a little too small root-mean-square radius. By applying the model to dibaryon search, similar results with QDCSM and ChQM are obtained. The results show that the hidden color channels are important for the NN intermediate-range attraction. The lattice QCD calculations obtained the stringlike multibody confinement interaction in the multiquark system [17]. It is equivalent to the two-body confinement Eq. (4) with $k = 1$ for a color singlet nucleon with three quarks. Oka extended the string-flip model to the six-quark system and obtained a reasonable description of NN interaction [11], which might be viewed as a modeling of the lattice QCD stringlike multibody confinement. QDCCM fits the NN scattering data better and we suspect it might be another modeling of the lattice QCD multibody confinement.

Certainly, one would expect to directly use the stringlike multibody interaction obtained in lattice QCD to calculate the NN interaction. However, it is not only because of the huge numerical task, but also because there is not any information about the transition interaction between different string structure, which hindered this approach.

Nuclear force is an old topic; it has been studied over 70 years and a large amount of experimental data has been accumulated. Although there are several approaches that can give almost perfect description of the experimental data, the mechanism for the intermediate-range attraction is still an open question. Lattice QCD achieved a qualitative description of the NN interaction already, and it will finally achieve a quantitative description. But, based on present lattice QCD technique, it can not reveal the physical mechanism, for example, to distinguish the phenomenological σ-meson exchange and the nucleon distortion similar to molecular covalent-bond mechanism for the intermediate-range attraction. One has to develop the nonperturbative continuous QCD field theory method as well as nonperturbative QCD model to explore the NN interaction.

[1] R. Machleidt, Adv. Nucl. Phys. **19**, 189 (1989) and references therein.

[2] E. Epelbaum, H. W. Hammer, and Ulf-G. Meissner, Rev. Mod. Phys. **81**, 1773 (2009) and references therein.

[3] A. Valcarce, H. Garcilazo, F. Fernandez, and P. Gonzalez, Rep. Prog. Phys. **68**, 965 (2005) and references therein.

[4] S. Aoki (HAL QCD Collaboration), e-print arXiv:1107.1284.

[5] A. Manohar and H. Georgi, Nucl. Phys. B **234**, 189 (1984).

[6] F. Wang, G. H. Wu, L. J. Teng, and T. Goldman, Phys. Rev. Lett. **69**, 2901 (1992).

[7] P. W. Anderson, Phys. Today **53**, 11 (2000).

[8] M. Ablikim *et al.* (BES Collaboration), Phys. Lett. B **598**, 149 (2004).

[9] N. Kaiser, S. Grestendorfer, and W. Weise, Nucl. Phys. A **637**, 395 (1998); E. Oset, H. Toki, M. Mizobe, and T. T. Takahashi, Prog. Theor. Phys. **103**, 351 (2000); M. M. Kaskulov and H. Clement, Phys. Rev. C **70**, 014002 (2004).

[10] L. Z. Chen, H. R. Pang, H. X. Huang, J. L. Ping, and F. Wang, Phys. Rev. C **76**, 014001 (2007).

[11] M. Oka and C. J. Horowitz, Phys. Rev. D **31**, 2773 (1985).

[12] K. Maltman and N. Isgur, Phys. Rev. D **29**, 952 (1984).

[13] D. R. Entem, F. Fernandez, and A. Valcarce, Phys. Rev. C **62**, 034002 (2000).

[14] G. H. Wu, L. J. Teng, J. L. Ping, F. Wang, and T. Goldman, Phys. Rev. C **53**, 1161 (1996); G. H. Wu, J. L. Ping, L. J. Teng *et al.*, Nucl. Phys. A **673**, 279 (2000); J. L. Ping, F. Wang, and T. Goldman, *ibid.* **657**, 95 (1999).

[15] J. L. Ping, H. R. Pang, F. Wang, and T. Goldman, Phys. Rev. C **65**, 044003 (2002); X. F. Lu, J. L. Ping, and F. Wang, Chin. Phys. Lett. **20**, 42 (2003).

[16] M. M. Xu, M. L. Yu, and L. S. Liu, Phys. Rev. Lett. **100**, 092301 (2008).

[17] C. Alexandrou and G. Koutsou, Phys. Rev. D **71**, 014504 (2005); F. Okiharu, H. Suganuma, and T. T. Takahashi, Phys. Rev. Lett. **94**, 192001 (2005).

[18] V. Dmitrasinovic, Phys. Rev. D **67**, 114007 (2003).

[19] M. Kamimura, Suppl. Prog. Theor. Phys. **62**, 236 (1977).

[20] R. A. Arndt, W. J. Briscoe, I. I. Strakovsky, and R. L. Workman, Phys. Rev. C **76**, 025209 (2007).

[21] J. L. Ping, H. X. Huang, H. R. Pang, F. Wang, and C. W. Wong, Phys. Rev. C **79**, 024001 (2009).

[22] M. Bashkanov *et al.* (CELSIUS-WASA Collaboration), Phys. Rev. Lett. **102**, 052301 (2009).

[23] R. A. Arndt, I. I. Strakovsky, R. L. Workman, and D. V. Bugg, Phys. Rev. C **48**, 1926 (1993).

[24] R. A. Arndt, L. D. Roper, R. L. Workman, and M. W. McNaughton, Phys. Rev. D **45**, 3995 (1992).

[25] M. P. Locher, M. E. Sainio, and A. Svarc, Adv. Nucl. Phys. **17**, 47 (1986).